Effect thickness of copper oxide thin films on structural, optical, electrical, and hydrophobic properties for use in self-cleaning technique

M. Zerouali[a,*], R. Daïra[a], B. Boudjema[a], R.Barillé[b], D. Bouras[c], S. Iaiche[d],
[a] Physico Chemistry of Surfaces and interfaces Research Laboratory (LRPCSI) ,University 20 august 1955-Skikda, P.B. 26, Road d'El-Hadaiek, 21000, Skikda, Algeria
[b]*MOLTECH-Anjou, University of Angers/UMR CNRS 6200, 2 Bd Lavoisier, 49045 Angers, France*
[c]*Laboratory of Active Components and Materials, University of Oum El Bouagh, Oum El Bouaghi, 04000, Algeria*
[d]*LASPI²A, University Abbes Laghrour – Khenchela 40000,Algeria*

In this work, copper oxide thin films were deposited by pneumatic spray pyrolysis method on a microscopy glass substrate, heated at 400°C for different deposition times (5min, 10min, 15min, 20min,25min, and 30min) using a 0.1M of precursor concentration. These films are characterized by X-ray diffraction (XRD), Fourier-transform infrared (FT-IR), spectroscopic ellipsometry, UV-visible spectroscopy, four points method, and water contact angle. According to the XRD, all peaks confirm the formation of the phase tenorite of the monoclinic structure. The deposited were polycrystalline copper oxide CuO with directions along (111) plane, the crystallites size between 14 and 23 nm. FTIR spectroscopy confirms the presence of the CuO phase and agrees that it will result in XRD. From the transmission spectra, the average transmission between 400 and 800nm is 65% to 50%, and the gap energy is 2.65 eV to 1.09 eV. The water contact angle values in all samples are greater than 90° and range from 96.4° to 103.2°, as we can see from these results that all the samples are hydrophobic films.

(Received August 22, 2023; Accepted November 8, 2023)

Keywords: Copper oxide, Thin films, Spray pyrolysis, Water contact angle, Hydrophobic films

1. Introduction

Scientific research and industrial development have paved the way for nanoscience and nanotechnology. The Nano technique It was a subject of extensive research for many years to this day. Nanotechnology is focusedonself-cleaning Several studies have been conducted in recent years on nanomaterials.Copper oxide is one of the attractive metal oxides for this technology, which is one of the most valuable materials due to its wide range of applications, such as gas sensors [1,2], antibacterial activity [3], solar cells [4] and photo catalysis [5].

Cuprous oxide (Cu_2O) and cupric oxide (CuO) are the two stable forms of copper oxide (CuO). These two oxides differencetheir colors, crystal formations, and physical characteristics. [6,7]. CuO is a monoclinic structure of the phase tenorite [8]. It is an extensively studied group II-VI [9]. With the lattice parameters a = 4.684 Å, b = 3.425 Å, c = 5.129 Å, and β= 99.28 Å.Is a p-type transition metal oxide semiconductor with a direct bandgap between 1.2 and 1.9 eV [10, 11]. Copper oxide has gotten much attention because of its non-toxicity, low cost [1], economy, good environmental adaptation [12], and high solar absorbance. It may thus be an excellent absorption material in solar cells [7, 13]. Copper oxide films have been prepared using various deposition techniques, such as pyrolysis spray [14], sol-gel [15], DC reactive sputtering [2], and thermal evaporation [16].

* Corresponding author: m.zerouali@univ-skikda.dz
https://doi.org/10.15251/DJNB.2023.184.1371

To find out the quality of the surface and the extent of the application of nanotechnology in self-cleaning, we used a water contact angle. She represents the angle formed between a liquid and a solid surface and measured only produced using pure liquids and very clean solid surfaces. If the liquid molecules are strongly attracted to the solid molecules, the drop will spread out fully over the solid surface, yielding a contact angle of 0°. Although an oxide layer or impurities on the solid surface can considerably increase the contact angle, this is typically the case for water on bare metallic or ceramic surfaces. The most prominent application of nanotechnology in household appliances is self-cleaning or easy-to-clean surfaces like the manufacture of water and stain-repellent clothing [17].

This work aims to develop single-phase structures of copper oxide in thin films of different spray times on a glass substrate. Then characterization of their structural, optical, and electrical properties. And in the end, we carry out an application in nanotechnology on the synthesized films as self-cleaning films and check the surfaces by the contact angle; as we can see from these results that all the samples are hydrophobic films which where opens up horizons for the field of nanotechnology thanks to their functional properties.

2. Experimental study

2.1. Preparation of thin layers

The copper oxide thin films are prepared by pneumatic spray pyrolysis method, with a flow rate of 20 ml/h for different spray times of 5 min, 10 min, 15 min, 20 min, 25 min, and 30 min, using copper nitrate precursor $Cu(NO_3)_2$ of molarity 0.1M, deposited on a glass substrate heated to 400°C.

3. Results and discussion

3.1. Thickness measurement

Figure. 1 shows the thickness of copper oxide (CuO) at different spraying times (t= 5, 10, 15, 20, 25, 30 min) by pneumatic spray pyrolysis method. It was observed that the thickness of these films changes between 102-650 nm. The thickness of our samples increases with the increase in spraying time.

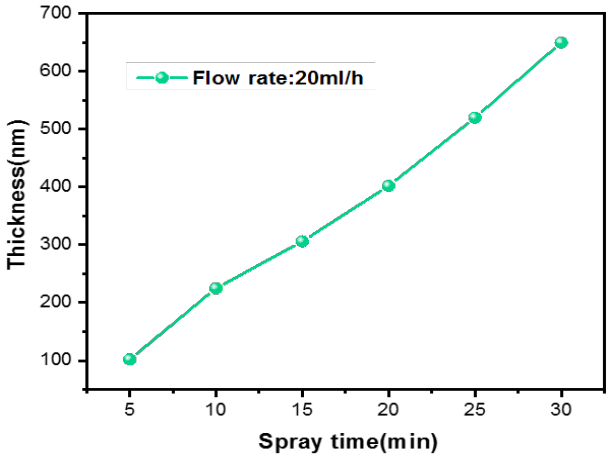

Fig. 1. Thickness of copper oxide as a function of spraying time.

3.2. X-Ray diffraction

DRX has identified the structural characteristics of copper oxide thin films for different spray times from 5 min to 30 min. As represented in (figure.2), we note the presence of several diffraction peaks at 2θ = 32.35°, 35.44°, 38.62°, 53.43°, 66.16° and 68.30° corresponding to the

following crystal planes (002),(110),(111),(020),(-311)and (220) respectively this is in good agreement with the JCPDS code 00-041-0254 which confirm the formation of the tenorite phase of the monoclinic structure. This reveals that the thin films are polycrystalline. In all the samples, a more intense peak corresponds to the (111) plane. It is generally reported that the CuO thin films represent a preferential orientation along the (111) plane; this result agrees with the bibliography [18,19]. When the spray time of copper nitrate was increased, it was found that the intensity of the two main peaks increased. The growth and crystallinity of the crystallites of these layers were improved. The increase in the intensity of the peaks confirms this.

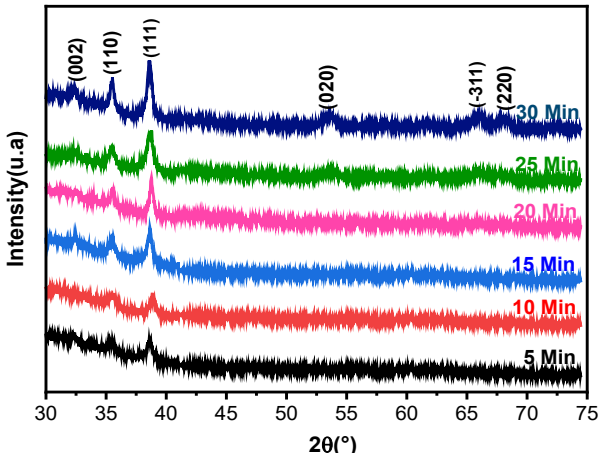

Fig. 2. XRD spectra of undoped CuO thin films deposited at 400 °C.

3.3. Texture coefficient

When determining the texture coefficient (Tc) and finding the preferred orientation of these films, equation (II.11) is used. Figure. 3 represents the variation of texture coefficient for the two planes (110) and (111) for the films of copper oxide at different spraying times. We notice that the texture coefficient in all the films (>1) in two planes (110) and (111) confirms the existence of a preferential orientation along the plane (110) and (111).

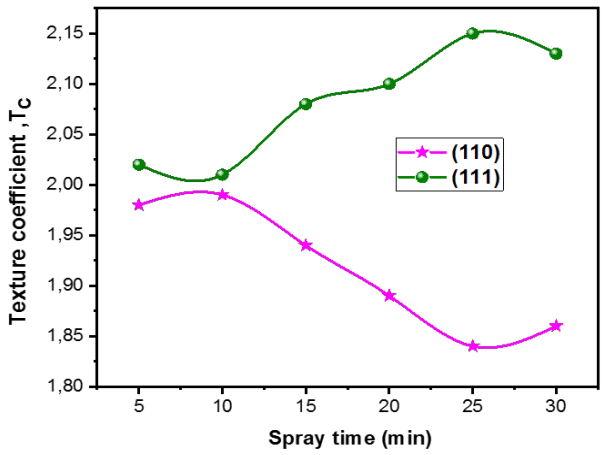

Fig. 3. Texture coefficient as a function of spraying time at (110) and (111).

3.4. Crystallite size and microstrain

The crystallite sizes of these layers are illustrated in Table 1, were calculated by Scherrer's equation [20]:

$$D = \frac{0.9 \cdot \lambda}{\beta \cdot \cos\theta} \quad (1)$$

where D is the size of the crystallites, λ is the wavelength of the incident ray,β is the width at half maximum (FWHM), and θ is the Bragg diffraction angle.

The microstrain ε was calculated by the following formula [21]:

$$\varepsilon = \frac{\beta \cdot cos\theta}{4} \quad (2)$$

The crystallites are nanometric sizes between 14 and 23 nm (Table 1). we note that the best sizes at 20 min in the time of spray. Figure.4 represents the curve of variation of the deformation andcrystallite size as a function of spray time; we note an inverse relationship between them. When the crystals are increased, the defects in the lattice decrease, which leads to a decrease in the microstrain in the crystal lattice of copper oxide.

Table 1. Lattice parameters of the samples.

Phases	Plane (hkl)	2θ (°)	FHWM β(°)	D (nm)	**ε** (10^{-4})	**δ**10^15 (Lines/ m^2)	a (Å)	b (Å)	C (Å)	**β**(°)	v ($Å^3$)
5min	(111)	38.62	0.543	14	22.36	5,10	4.68	3.41	5.14	99.20	80.79
10min	(111)	38.85	0.503	15	20.7	4,44	4.68	3.42	5.13	99.25	81.29
15min	(111)	38.62	0.452	17	18.61	3,46	4.68	3.41	5.14	99.12	81.30
20min	(111)	38.76	0.342	23	14.08	1,89	4.66	3.43	5.14	99.71	81.14
25min	(111)	38.63	0.483	16	19.89	3,90	4.63	3.42	5.14	99.19	80.38
30min	(111)	38.61	0.373	21	15.36	2,26	4.64	3.43	5.14	98.99	80.85

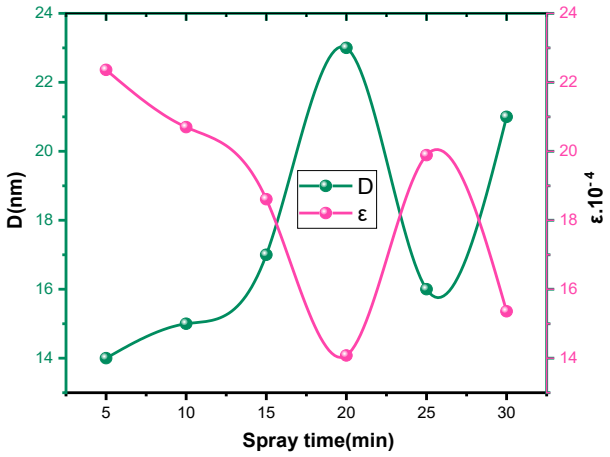

Fig. 4. Crystallite size and microstrain of the films as a function of spray time.

3.5. Vibration spectroscopy investigations using FT-IR

The ATR-FTIR spectroscopy technique was used to characterize the generated thin films to understand better the chemical compositions of the samples and the interactions that determine their properties. For different spray times, infrared (IR) spectra of CuO thin films were recorded in the range 400-2500 cm-1, as shown in (figure 5). Several absorption bands were clearly identified.

The peaks at 413 cm^{-1}, 424 cm^{-1},462 cm^{-1},478 cm^{-1},529 cm^{-1},575cm^{-1},478 cm^{-1},529 cm^{-1},718 cm^{-1}, 908 cm^{-1} are characterized as the Cu-O bond and another author's bonde of 1540cm^{-1}, 1650 cm^{-1} corresponding to the vibration of the O-H bond which is associated with the vibrational mode of the hydroxyl groups bonded to the adsorbed water. These results are in good agreement with references [22, 23, 24].

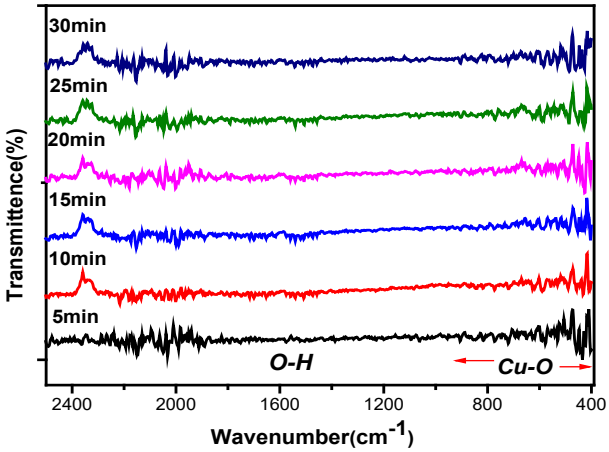

Fig. 5. ATR-FTIR spectra of copper oxide thin films for different spray times.

3.6. Optical properties

3.6.1. Transmittance spectra

Figure 6 shows the transmittance spectra of CuO obtained at different spray times in the wavelength range (200 nm to 900 nm). From this figure, we notice that the transmittance increases with the increase of the wavelength in the whole sample. We distinguish two regions; one region has an average transmittance greater than 50%, and the maximum transmittance is about (65%) in the wavelength region above 500 nm, and another region in the visible of strong absorption by what the energy of the incoming photons is close to the edge of absorption (energy value of band forbidden) also corresponding to the fundamental absorption (λ<500nm), for which the transmittance is canceled about below 400nm. This transition wavelength corresponds to the optical gap energy of the copper oxide layers studied. All the photons of energy higher than the gap (and thus all the photons having a wavelength lower than 500 nm) are absorbed instead of being transmitted. This absorption is due to the interband electronic transition. The variation of the transmission in this region is exploited to determine the gap.

On the other hand, we observe a shift of the absorption threshold towards low energies (long wavelengths). This shift is attributed to the increase in the concentration of free carriers in the material [25]. The spray time of 5min represented a good transmittance in the visible range accused of the lower thickness.

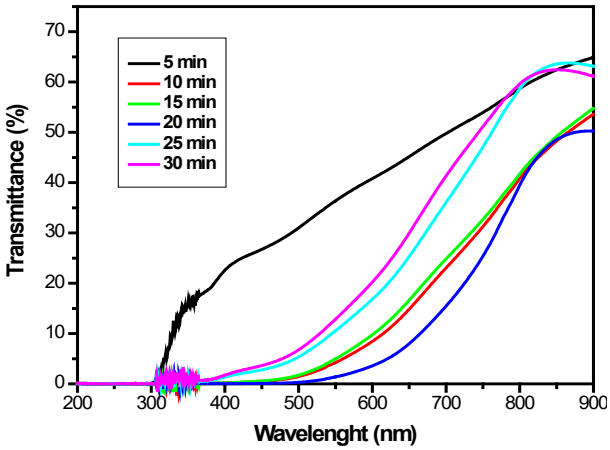

Fig. 6.Variation of the transmittance of CuO films deposited at different Spray times.

3.6.2. Gap energy

To determine the gap energy of the thin layers of samples prepared by the spin-coating method, the following tauc relation is used [26]:

$$\alpha h\nu = A \cdot \left(h\nu - E_g\right)^{1/2} \tag{3}$$

with A: Constant, Eg: Optical Gap in eV, hν: The energy of a photon eV.

Figure 7 shows the plot of $(\alpha h\nu)^2$ as a function of the energy of a photon $h\nu$, and by the extrapolation method, we have represented the optical gap E_g.

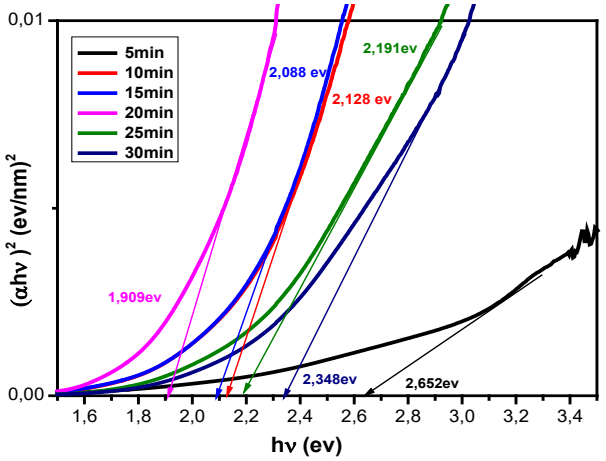

Fig. 7. Variation of $(\alpha h\nu)^2$ as a function of the Photon energy of copper oxide for different spray times.

Several factors affect the gap energy values, like the spray times and the thickness. Figure 8 represents the variation of the gap energy as a function of spray time. We notice a decrease and an increase in the optical gap such that the values of the gap energy varied between 2.652 eV and 1.909 eV. The spray time 20 min represents the minimum value of the gap energy. This can be explained by a good crystallization of our material, which confer the large size of crystallites obtained for this spray time. Also, the low transmittance indicates the amount of material deposited.

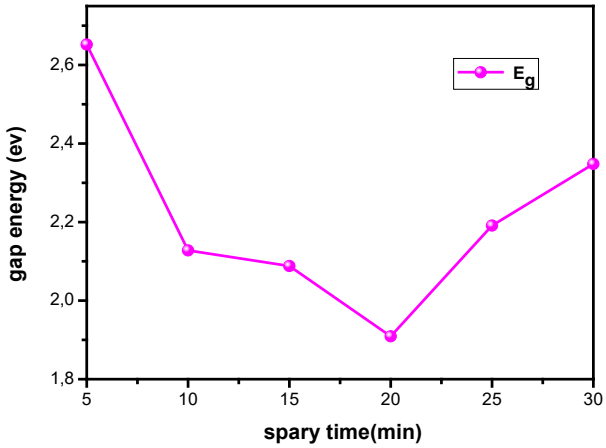

Fig. 8. Variation of the gap energy as a function of the spray time.

3.7. Optical constants

Using a spectroscopic ellipsometer, we obtained these constants

3.7.1. Refractive index (n)

Figure 9 shows the refractive index spectra as a function of photon energy for different spray times. The increase in the refractive index is related to the increase of the packing density as a result of the improvement of the crystal structure of the prepared copper oxide films in the case of spray times of 5min and 20min. The values of the refractive index increase gradually with the increase of the photon energy lower than the value of the gap energy of these films. Then after the values of gap energy, there is a decrease in the refractive index due to the high value of optical absorption due to direct electronic transmissions.

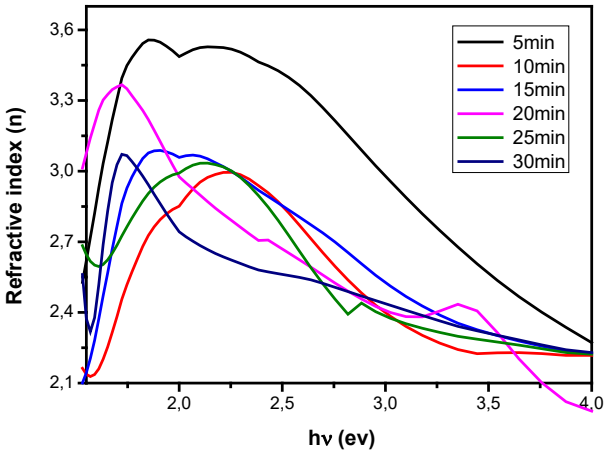

Fig. 9. Refractive index of CuO thin films deposited at different spray times.

3.7.2. Extinction coefficient (K)

The extinction coefficient is defined as the amount of energy storedby the electrons of the layer material. Figure 10 represents the variation of the extinction coefficient as a function of photon energy for different spray times of thin films of copper oxide. This increase is due to the rapid increase of the absorption coefficient at these energies, which may indicate the appearance of direct electronic transitions. This phenomenon can be explained by the values of the absorption coefficient change; therefore, the extinction coefficient is related to the absorption coefficient. The

spray time taken into account from the curves is clear. The spray time affects the absorption properties and the extinction coefficient.

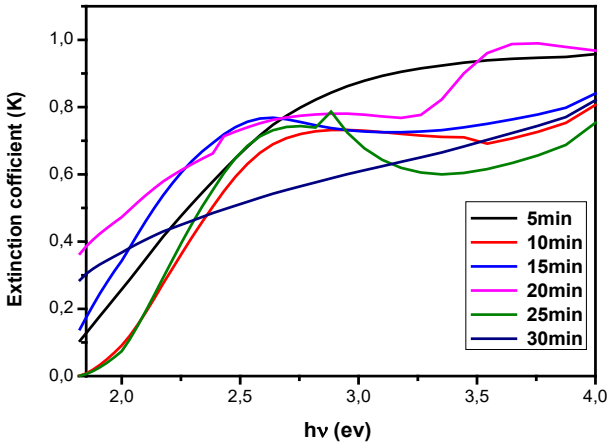

Fig. 10. the variation of the extinction coefficient as a function of photon energy for different spray times of CuO.

3.7.3. Dielectric constant (ε)

The dielectric constant is a fundamental optical parameter and is written as:

$$\varepsilon = \varepsilon_1 - i\varepsilon_2 \tag{4}$$

where ε_1 is the real part of the dielectric constant, which is related to the energy stored in the material, and ε_2 is the imaginary component of the dielectric constant, which is related to the energy dissipation in the material [27].

3.7.3.1. Real part of dielectric constant (ε_1)

The real part of the dielectric constant is calculated from the following relation.

$$\varepsilon_1 = n^2 - k^2 \tag{5}$$

The following spectra show the variation of the real part of the dielectric constant as a function of the energy of a photon. It can be seen from Figure11 that the values of the real dielectric constant increase progressively with the increase of the photon energy and then decrease sharply in the high energy range for all the prepared films. It is obvious that the curves are similar to the refractive index curves due to the dependence of the values of the real part of the dielectric constant on the values of the refractive index according to equation (5) on the extinction coefficient values. As we can see, the extinction coefficient's effect is very small compared to the effect of the refractive index, so it can be neglected, especially at low photon energies.

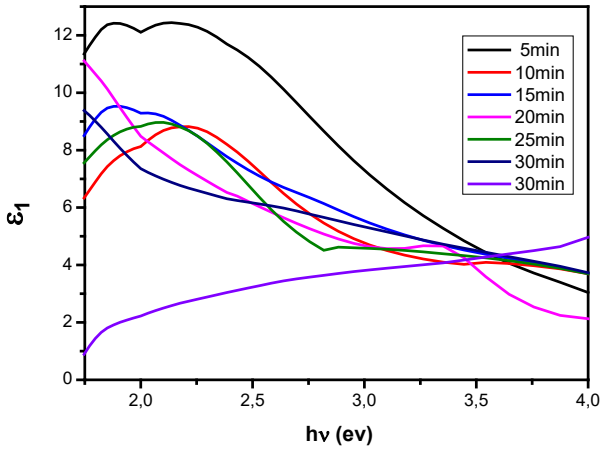

Fig. 11. Variation of the real part of the dielectric constant as a function of the energy of a photon.

3.7.3.2. Imaginary part of dielectric constant (ε_2)

The imaginary part of the dielectric constant is calculated from the following relation

$$\varepsilon_2 = 2nk \tag{6}$$

The variation of the imaginary part of the dielectric constant as a function of the incident photon energy with the evolution of the spray time is represented in figure (12) as it is noted that the imaginary part of the dielectric constant almost increases with the increase of the spray time. The increase of the absorption energy shows this increase. This result is in good agreement with the extinction coefficient results. In all films, the peaks of the curves creep towards low photon energies (long wavelengths), and note also the 5min spray time film is shown the value one as the highest value of the imaginary dielectric constant.

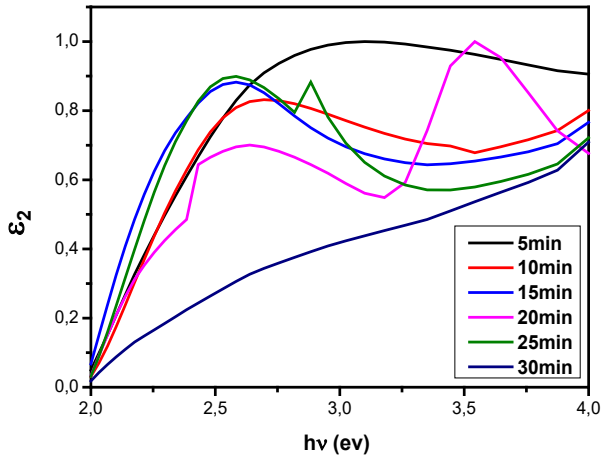

Fig. 12. Variation of the imaginary part of the dielectric constant as a function of the energy of a photon.

3.8. Electrical properties

The four-point method can measure the electrical conductivity (σ) and resistivity (ρ) of CuO oxide thin films obtained by spray time deflection. The results are presented in the following table.

Table 2. Electrical parameters obtained by the 4-point method.

Spray time (min)	Resistivity (Ω .cm)	Conductivity ($\Omega^{-1}.cm^{-1}$)
5	4783.649	$2.1.10^{-4}$
10	3325.678	3.10^{-4}
15	3202.561	$3.1.10^{-4}$
20	2.938	0.34
25	48.936	0.0204
30	220.826	0.00458

The variation of electrical conductivity and resistivity as a function of spray time is presented in the following figure.

We notice a decrease and an increase of the electrical conductivity with the increase of the spray time until obtaining a maximum value of 0.34 Ω^{-1} .cm^{-1}, corresponding to the time of spray 20min. This result is in agreement with the results of reference [28]. And the other electrical conductivity values agree with the references [14, 29]. The increase in electrical conductivity is well related to the increase in free charge carriers and the decrease in crystalline defects due to the increase in crystal size compared to the others. These results of the electrical conductivity are well-tuned with the results of the gap energy such that when the gap energy decreases, the electrical conductivity increases. The decrease of the electrical conductivity is related to the decrease of the crystallite size and, therefore, the presence of grain boundaries and defects that can be increased to the optical gap energy.

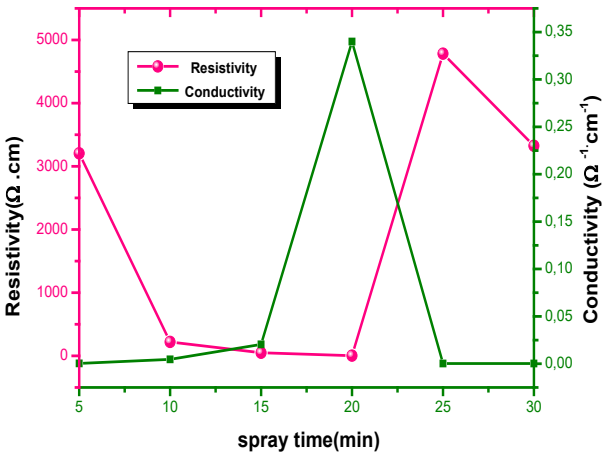

Fig. 13. Variation of conductivity and resistivity as a function of spray time.

3.8. Water contact angle

The contact angle of the water droplets depends on the structure of the surfaces and the variation of the size of the water droplets at the nanoscopy scale. As represented in the following images.

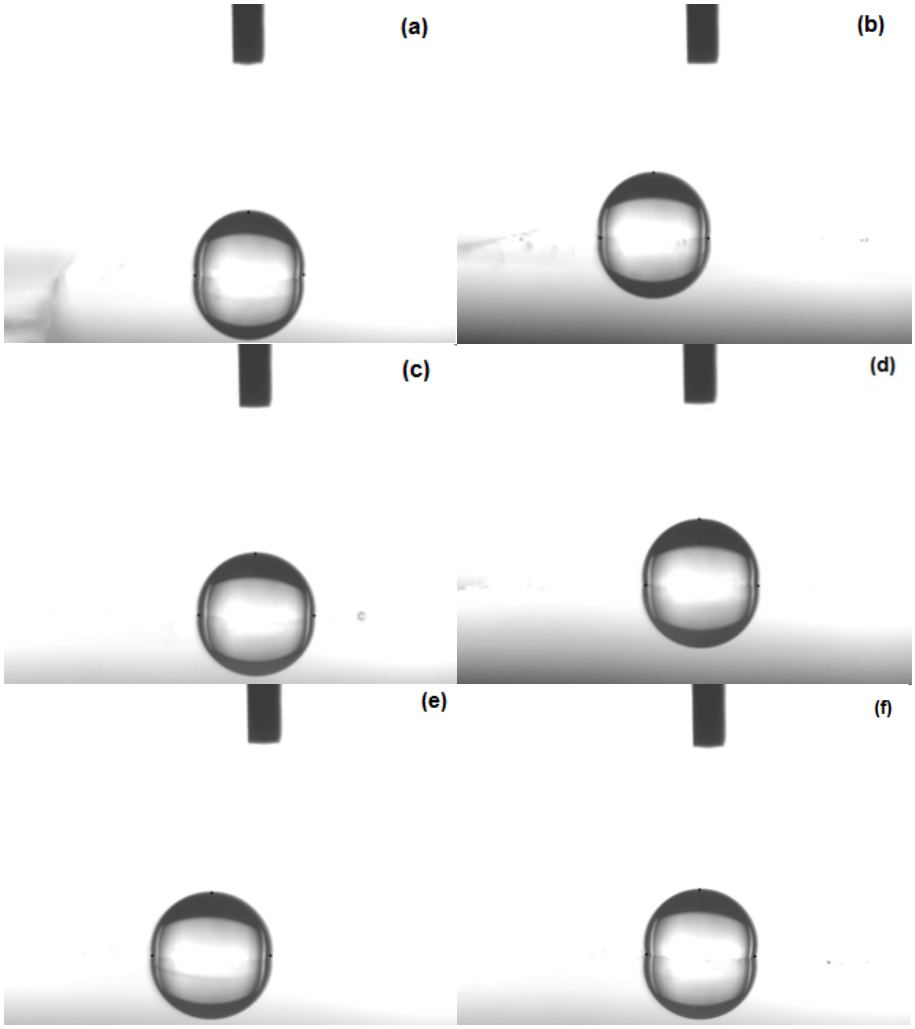

Fig. 14.Water contact angle image of various spray times of CuO (a),5 min (b),10 min (c),15 min (d),20 min (e),25 min (f),30 min.

Figure (15) represents the variation of the contact angle as a function of spray time, which corresponds to a change in the thickness of the samples. We notice an increase and decrease of the contact angle such that their values in all the sample is greater than 90° and varied between 96.4°and 103.2°. The contact angle on the rough surface is greater than on the smooth surface, indicating that the roughness of the solid hydrophobic improves its hydrophobicity [30-36]. Generally, suppose the contact angle with water is less than 90°. In that case, the solid surface is considered hydrophilic, and if the contact angle with water is greater than 90°, the solid surface is considered hydrophobic [17]. The lowest contact angle is observed for the 15min spray temples. This is due to the increased water adsorption on the film surface due to its smooth surface. As we can see from these results, all the samples are hydrophobic films, which open horizons for nanotechnology, such as the manufacture of waterproof fabrics.

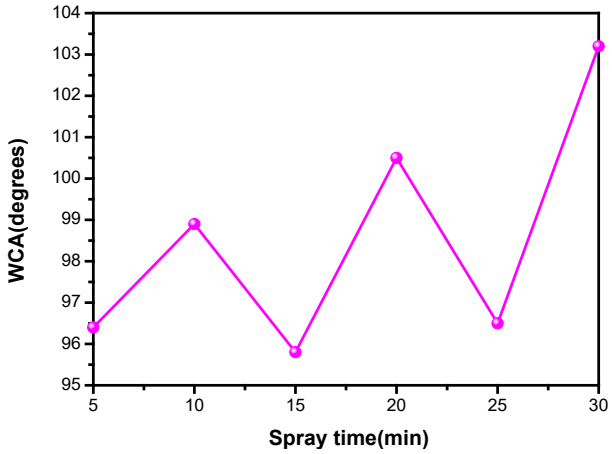

Fig. 15.Variation of water contact angleas a function of various spray times.

Acknowledgments

This work has been supported by the Laboratory of Research on the Physico-Chemistry of Surfaces and Interfaces (LRPCSI), 20 Août 1955 University -Skikda, Algeria and Laboratory of MOLTECH-Anjou, University of Angers/UMR CNRS 6200, 2 Bd Lavoisier, 49045 Angers, France.

4. Conclusion

Thin layers of CuO for different deposition times were used in nanotechnology as self-cleaning thin films. These films were deposited on a glass substrate by the pyrolysis spray method. According to XRD data, the films produced were polycrystalline with a C2/c space group. The water contact angle results show that all the samples are hydrophobic films with a contact angle that increases with increasing layer thickness. This means there is an inverse relationship between the contact angle and the thickness of the layer. Also, the contact angle on the rough surface is greater than on the smooth surface. This indicates that the roughness of the hydrophobic solid improves its hydrophobicity.

References

[1] L. Sun et al., Adv. Energy Mater., vol. 9, no 48, p. 1-11, 2019 ; https://doi.org/10.1002/aenm.201902839

[2] H. Search, C. Journals, A. Contact, M. Iopscience, I. P. Address, Sputtered copper oxide (CuO) thin films for gas sensor, vol. 2417, p. 0-4, 2006.

[3] D. Rania, A. Rabah, T. Mamadou, M. Christine, Elaboration de nanomatériaux fonctionnels pour des applications biomédicales, p. 1-10, 2017.

[4] T. Oku, R. Motoyoshi, K. Fujimoto, T. Akiyama, B. Jeyadevan, J. Cuya, J. Phys. Chem. Solids, vol. 72, no 11, p. 1206-1211, 2011 ; https://doi.org/10.1016/j.jpcs.2011.06.014

[5] A. O. Ibhadon, P. Fitzpatrick, Heterogeneous Photocatalysis: Recent Advances and Applications, p. 189-218, 2013 ; https://doi.org/10.3390/catal3010189

[6] R. P.Wijesundera, M. Hidaka, K. Koga, J. Y. Hoi, N. E. Sung, Ceram. - Silikaty, vol. 54, no 1, p. 19-25, 2010.

[7] L. J. Meenakshi, B. R. Aswathy, P. K. Manoj, AIP Conf. Proc., vol. 2287, no 11, p. 698-701, 2020 ; https://doi.org/10.1063/5.0029961

[8] J. Chen, B. J. Hansen, G. Lu, J. Nanomater., vol. 2008, no 1, 2008 ; https://doi.org/10.1155/2008/830474

[9] G. Madec, P. Delecluse, M. Imbard, et C. Levy, Notes du Pôle Modélisation, Inst. Pierre Simon Laplace, vol. 14, no 4, 2014 ; https://doi.org/10.2478/adms-2014-0021

[10] M. Asadi, S. M. Rozati, Mater. Sci. Pol., vol. 35, no 2, p. 355-361, 2017 ; https://doi.org/10.1515/msp-2017-0054

[11] M. T. S. Nair, L. Guerrero, O. L. Arenas, P. K. Nair, Appl. Surf. Sci., vol. 150, no 1, p. 143-151, 1999 ; https://doi.org/10.1016/S0169-4332(99)00239-1

[12] R. D. Prabu et al., Mater. Sci. Semicond. Process., vol. 74, no October 2017, p. 129-135, 2018 ; https://doi.org/10.1016/j.mssp.2017.10.023

[13] G. Applications et A. Rydosz, The Use of Copper Oxide Thin Films in Gas-Sensing Applications , 2018.

[14] S. Kose, F. Atay, V. Bilgin, I. Akyuz, Some physical properties of copper oxide films : The effect of substrate temperature , vol. 111, p. 351-358, 2008 ; https://doi.org/10.1016/j.matchemphys.2008.04.025

[15] F. Aksoy, G. Akgul, N. Yildirim, H. Emrah, Mater. Chem. Phys., vol. 147, no 3, p. 987-995, 2014 ; https://doi.org/10.1016/j.matchemphys.2014.06.047

[16] K. K. H. S. Z. Sadeghi, A comparative investigation on growth, nanostructure and electrical properties of copper oxide thin films as a function of annealing conditions, 2014.

[17] A. James et al., Determination of Contact Angle for Various Fluids Used in Industries, vol. 6, no 2, p. 30-31, 2017.

[18] R. Djebian, B. Boudjema, A. Kabir, C. Sedrati, Solid State Sci., vol. 101, no February, p. 106147, 2020 ; https://doi.org/10.1016/j.solidstatesciences.2020.106147

[19] S. D. Al Ghamdi, A. O. M. Alzahrani, M. S. Aida, M. S. Abdel-wahab, J. Mater. Sci. Mater. Electron., vol. 33, no 18, p. 14702-14710, 2022 ; https://doi.org/10.1007/s10854-022-08390-8

[20] F. Bayansal et T. Tas, Effect of Cobalt Doping on Nanostructured CuO Thin Films, no Ii, 2014 ; https://doi.org/10.1007/s11661-014-2306-1

[21] M. Science-Poland, Fabrication and characterization of Zn doped CuO nanofiber using newly designed nanofiber generator for the photodegradation of methylene blue from textile effluent, vol. 36, no 3, p. 520-529, 2018 ; https://doi.org/10.2478/msp-2018-0056

[22] M. Serhan et al., AIChE Annu. Meet. Conf. Proc., vol. 2019-Novem, 2019.

[23] B. T. Sone, A. Diallo, X. G. Fuku, A. Gurib-Fakim, M. Maaza, Arab. J. Chem., vol. 13, no 1, p. 160-170, 2020 ; https://doi.org/10.1016/j.arabjc.2017.03.004

[24] C. Chimeno-Trinchet, A. Fernández-González, J. Á. García Calzón, M. E. Díaz-García, R. Badía Laíño, Sci. Technol. Adv. Mater., vol. 20, no 1, p. 657-672, 2019 ; https://doi.org/10.1080/14686996.2019.1621683

[25] A. Boughelout, A. Bensouilah, L. Chabane, N. Zebbar, et A. H. M. Kechouane, Les proprietes optiques et electriques des couches minces de zno deposees par pulverisation cathodique a basse pression, vol. 9075, 2008.

[26] Z. Madiha, D. Radouane, B. Dikra, B. Boudjema, and R. Barille , J. Nano Res., vol. 80, pp.1–19, 2023.

[27] N. Y. Mostafa, A. Badawi, et S. I. Ahmed, «Results Phys., vol. 10, no April, p. 126-131, 2018 ; https://doi.org/10.1016/j.rinp.2018.05.030

[28] F. Z. Chafi, L. Bahmad, N. Hassanain, B. Fares, L. Laanab, A. Mzerd, arXiv, p. 1-13, 2018.

[29] H. Hashim, S. S. Shariffudin, P. S. M. Saad, H. A. M. Ridah, IOP Conf. Ser. Mater. Sci. Eng., vol. 99, no 1, 2015 ; https://doi.org/10.1088/1757-899X/99/1/012032

[30] J. Y. Park, M. Y. Ha, H. J. Choi, S. Do Hong, H. S. Yoon, J. Mech. Sci. Technol., vol. 25, no 2, p. 323-332, 2011 ; https://doi.org/10.1007/s12206-010-1218-2

[31] R.Daira, B.boudjema, Journal of intense pulsed lasers and applications in advanced physics, Vol. 5, No. 1, (2015), p. 1- 4.

[32] R. Daira, B. Boudjema, M. Mordjaoui, M. Mezéri, Optoelectron. Adv. Mat. **5**(2), 167 (2011).

[33] R. Daira, B. Boudjema, A. Mohamoudi, Chalcogenide Letters, 20(4) pp.277-284 (2023) ; https://doi.org/10.15251/CL.2023.204.277
[34] R. Daira B. Boudjema, M. Bououdina, M. S. Aida, Applied Science, (2023) ; https://doi.org/10.3390/app13148193
[35] R. Daira, B. Boudjema, journal Of Intense Pulsed Lasers and Applications in Advanced Physics, 5 (2015).
[36] R. Daira, S. Regaie, B. Boudjema, A. Harrouz, Algerian Journal of Renewable Energy and Sustainable Development, 5 (1) (2023) ; https://doi.org/10.46657/ajresd.2023.5.1.10